**Adam ŚWITOŃSKI[1,2], Tomasz BŁACHOWICZ[3], Marta MISIUK-HOJŁO[4], Konrad WOJCIECHOWSKI[1,2]**

Polish-Japanese Institute of Information Technology, Faculty of Bytom *(1),*
Silesian University of Technology, Faculty of Automatic Control, Electronics and Computer Science *(2),*
Silesian University of Technology, Institute of Physics *(3), Wrocław Medical University, Department of Ophthalmology (4),*

# Supervised and unsupervised segmentation of multispectral retina images

***Streszczenie.*** *W pracy zaprezentowano metodę segmentacji wielospektralnych obrazów dna oka ukierunkowaną na diagnostykę schorzeń jaskry i retinopatii cukrzycowej. Akwizycja wielospektralna prowadzona jest w 21 oknach widma z zakresu 400nm do 740nm na bazie elektronicznie sterowalnego filtra ciekłokrystalicznego i wysokiej czułości monochromatycznej kamery CCD. Przedstawiono uzyskane wyniki segmentacji w podejściu nadzorowanym i nienadzorowanym (**Nadzorowana i nienadzorowana segmentacja wielospektralnych obrazów dna oka**).*

***Abstract.*** *The segmentation method of multispectral human eye images suitable in ophthalmic diagnosis of structural retinal features characteristic for glaucoma and diabetic retinopathy diseases is presented. A multispectral imaging was realized in 21 spectral windows, between 400nm and 740nm, on a base of liquid crystal tunable filter and a high sensitivity monochrome camera. Results of supervised and unsupervised segmentation procedures of retina images, adopted from a color fundus device, are presented.*

**Słowa kluczowe**: obrazowanie wielospektralne, nadzorowane i nienadzorowane uczenie maszynowe, diagnostyka chorób dna oka. segmentacja obrazów wielokanałowych
**Keywords**: multispectral imaging, supervised and unsupervised machine learning, retina diagnosis, segmentation of multichannel images

## Introduction

Information captured in multispectral regime overcomes many limitations of electromagnetic radiance intensities stored directly in a conventional set of red, green and blue (RGB) detectors. RGB standard tries to follows human retina photoreceptors capabilities, however in practice, it is not able to restore exactly a rich set of colors perceptible by a human brain. Nowadays, multispectral imaging is widely used in laboratory works as well as in applied studies - let's mention examples from medicine [1], geology [2], agriculture [3], or art [4].

Since multispectral image information overpasses human sensing capabilities, then it requires appropriate data reduction to match requirements of a given application. There are two main subsequent steps managing rich set of multispectral data. First, it bases on spectral components reduction, using for example PCA [5-7], KPCA [8], and ICA [9,10] methods, in order to project multidimensional images onto 3-dimesnional color space, equivalent to RGB standard. Second, a perception of vast multispectral data can be significantly enhanced by use of proper segmentation algorithms. Recently, segmentation is intensively applied in OCT diagnosis for 3-dimensional imaging of human retina [11]. It employs different specific solutions based on graph theory and dynamic programming for closed-contour structural features recognition [12], or can adopt energy-minimizing active scheme applied for contours segmentation with no edges [13], or finally, it segments OCT images by machine learning approach based on global image descriptors formed from multi-scale spatial pyramid [14].

Our multispectral experiments were carried out with the single-photon sensitive thermoelectrically cooled Luca$^{EM}$ S DL-658M camera manufactured by Andor Technology, and computer-controlled VariSpec$^{TM}$ liquid-crystal (LC) tunable filter manufactured by Channel Systems Inc. The idea of the setup is given in Fig. 1. The camera provides 658x496 (VGA) active CCD pixels resolution, up to 37.2 fps frame rate, and the quantum efficiency between 40-50 % in the visible 400-700nm range. The LC filter offers 50ms response time, the bandwidth in the range of 7-20nm, and the transmission outside the pass-band less than 0.01%. The pass-band can be swept continuously in the 400-720nm range.

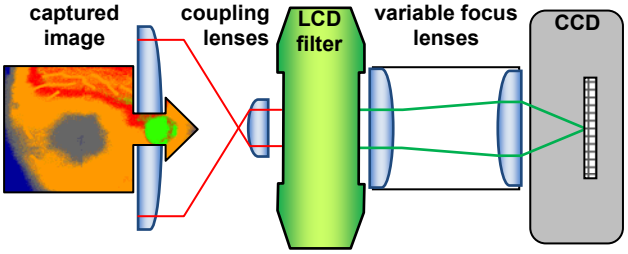


Fig. 1 The scheme of experimental setup.

What is proposed here is a description of algorithms in quite general style, since future, specific implementations can employ different methods of image processing. We indicate only onto the steps which are sufficient for effective segmentation of multispectral images for the presented device.

## Image segmentation

The outlines of the proposed methods, for multispectral image segmentation, are given in Fig. 2. Thus, the two approaches are considered here: firstly, the unsupervised-automatic procedure, and secondly, the semi-automatic supervised method which requires user interaction and control. The common steps for both approaches are as follows: noise filtering, signature extraction, spectrum normalization, and image post-processing.

**Denoising:** At the beginning, before analysis of specific image, in order to access desired information, it is necessary to reduce noise registered during capturing process. It is extremely troublesome problem, due to a relatively narrow spectral transmittance of LCD filter, which results in very low-level registered intensities for a given wavelength. Classical methods based on a low pass filtering, i.e. Gaussian blurring and median filtering, usually solve this problem [15].

**Signature Extraction:** The next step, a signature extraction, determines spectral signatures (intensities as a function of registered wavelength) of an every imaged pixel. From that moment an image is further represented by a set of points described rather by their spectral properties, not by the multispectral device channels

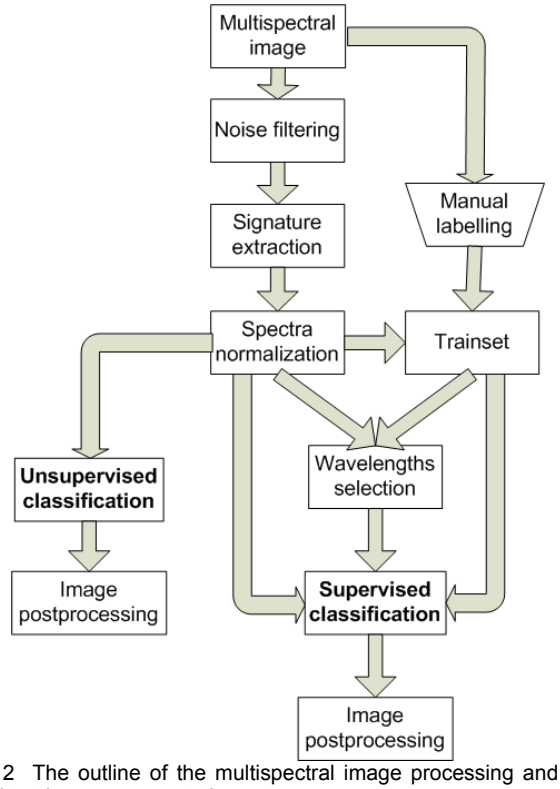


Fig. 2 The outline of the multispectral image processing and the resultant image segmentation.

**Normalization:** Thus, recorded spectral intensities strongly depend on represented wavelengths and the image local information. It results from a non-uniform spectral characteristic of the LCD filter and irregular lighting conditions. To normalize spectral information, and to minimize such dependencies, the spectral normalization should be carried out. Typically, the two normalization approaches can be realized. The first method is based on separate normalization of an every wavelength for different pixels (wavelength-based normalization), marked here as WN, while in the second method, spectral vectors are calculated for an every pixel and different spectral channels (pixel-based normalization) [16], marked in the following sections as PN.

A typical WN spectrum is fitted to (0,1) range in a linear way. It means that the smallest and greatest values of spectral components are determined for a considered image, and the linear scaling on intensities $I^{WN}(x,y,\lambda)$ can be expressed as follows

$$I^{WN}(x,y,\lambda) = s(x,y)\cdot\left[I(x,y,\lambda) - c(x,y)\right] \tag{1}$$

where $s(x,y) = \max_{\lambda}\left[I(x,y,\lambda)\right] - \min_{\lambda}\left[I(x,y,\lambda)\right]$, and $c(x,y) = \min_{\lambda}\left[I(x,y,\lambda)\right]$.

In a PN approach, spectrum components form a vector, which is resized to default unit length in following way

$$I^{PN}(x,y,\lambda) = \frac{I(x,y,\lambda)}{\left\|I(x,y,:)\right\|} \tag{2}$$

where $\left\|I(x,y,:)\right\|$ is the spectrum norm. Usually, the Euclidean metric

$$\left\|I(x,y,:)\right\| = \sqrt{\sum_{\lambda} I^2(x,y,\lambda)} \tag{3}$$

can be employed to complete this step. The PN normalization offers choice of vector direction which points onto needed spectral feature, independently from an externally applied non-uniformly distributed light intensity.

Apart from the above, the normalization can be improved by calibration of capturing device to a specified spectral scale. During calibration process transformation between spectral scale of the device and referenced spectral scale is determined. If physical properties of both spectral scales are not known directly, then a supervised machine learning should be applied. It requires preparation of a representative training set, containing corresponding spectral instances for the scales. To fulfill this postulate we used multispectral photographs of GretagMacbeth ColorChecker with defined spectral components of its colors. Details about such linear transformations can be found in [17], while nonlinear kernel based transformations are described in [18,19].

**Classification, Segmentation and Associated Reconstruction:** Before finalizing an image preprocessing, spectral signatures can be grouped (clustered) by unsupervised classification [17] using a given unsupervised segmentation approach, for example, the Waikato Environment for Knowledge Analysis (WEKA), which is a comprehensive suite of Java class libraries [20]. A classifier choice and its numerical initialization method choice are crucial decisions, since a number of interest group have to be specified in an image. Next, during reconstruction of segmented image, the connected components of the pixels belonging to the same classified group are determined. They form regions of segmentation process (comp. Fig. 4., where unsupervised pixels of a different groups are represented by different colors).

**Postprocessing:** Finally, a postprocessing step, which is common for unsupervised and supervised approaches, removes small insignificant regions and smoothes contours. Especially, in many situations the morphological open-close filtering [15], which employs specified size of structural element, rectangular or circular in shape, works effectively. Importantly, in order to reduce effectively adverse effects, the open-close filtering can be is iterated for the different sizes of structural element.

**Supervised segmentation:** In supervised segmentation a training set, containing spectral signatures with specified class identifiers, has to be supplied. It is prepared by a manual choice of interested image regions. It can be assumed that only a few lines marked by a brush tool for an every class is sufficient [17].

**Wavelength Selection:** Automatic, supervised feature selection of spectral wavelengths removes from spectral signatures wavelengths containing only noise and the wavelengths which do not discriminate objects specified by the training set. This procedure forms simpler and more clear signatures, thus the consecutive classification should be easier. Next, the reduced spectral signatures are further labeled by supervised classification with a supplied training set. Similarly to unsupervised segmentation, the associated components of pixels, belonging to a given class, are postprocessed by a morphological filtering. The advantage of the supervised segmentation approach results from the fact that the assigning of classes to regions is determined by a training set .

**Disscussion of results**

In Fig. 3 selected multispectral images in the form of separate spectral channels are presented. The results of unsupervised segmentation by 'Fuzzy KMeans clustering, with different number of clusters, are shown in Fig. 4. The median filtering and PN normalization are performed before

clustering. The use of two clusters creates some boundaries of the optic disc, however the optic disc and the retina are not separated significantly. The segmentation is more accurate with greater number of clusters, when for instance, the yellow spot region is revealed. This causes, however, improper division of anatomical structures and can be observed, for a retina region, as different clusters. Thus, the segmented image requires further processing to identify segmented regions.

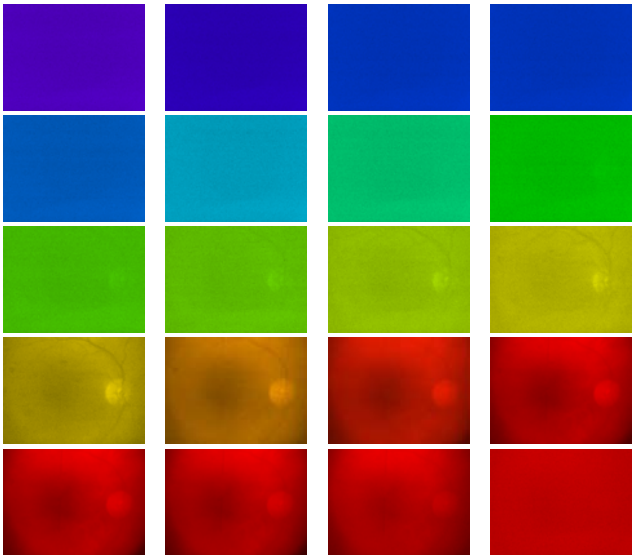

Fig. 3 Input set of images of the human eye retina. The images captured for the following wavelengths (left-to-right, up-to-down, values in *nm*): 416, 432, 448, 464, 480, 496, 512, 528, 544, 560, 576, 592, 608, 624, 640, 656, 672, 688, 704, 720. In right part of an image the optical disk is clearly seen.

The training set used in supervised approach is visualized in Fig. 5. It contains manually labeled regions of the optical disc, yellow spot and an outside region. It is made by a windows software-brush tool. The chosen spectral signatures, with attributes obtained after WN and PN normalization, are reduced by a supervised feature selection with Greedy Hill Climbing search and wrapper subset evaluation followed by the Bayes classification [20]. The results shown in Fig. 6a and Fig. 6b are very promising. The optic disc and yellow spot regions are detected precisely. There are some small missclassified regions of the yellow spot, located on the left side of the retina. However, this can be easily corrected by determination of the Greatest Connected Component analysis [20] of the yellow spot.

In summary, we would like to emphasize that, we avoid estimation of numerical measures of segmentation quality using such descriptors like: 'true positives', 'true negatives', 'false positives', 'false negatives'. Additionally, medical experts usually do not use analysis of multispectral channels - they are trained only for color fundus camera eye images.

Our contribution focuses on the construction of the multispectral imaging device for retinal diagnosis in global spectral spaces, out of RGB scheme. The prototype device allows us to acquire spectral data of the retina at the acceptable level of noise. The acquisition takes place in very difficult conditions because of the eye movements. However, the only spectral data of image pixels are sufficient for detection of basic anatomical structures. Importantly, our approach does not take into consideration local properties of pixels neighborhood.

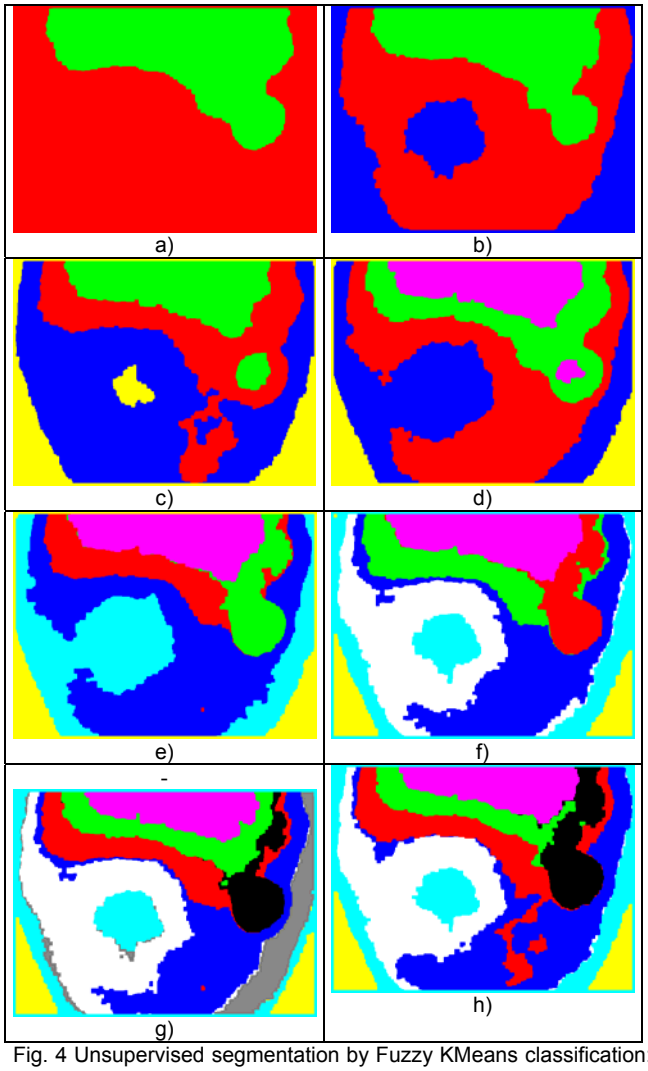


Fig. 4 Unsupervised segmentation by Fuzzy KMeans classification: a) two classes b) three classes c) four classes d) five classes e) six classes, f) seven classes, g) eight classes, h) nine classes.

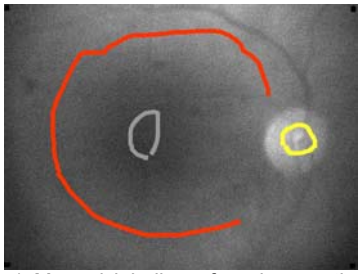

Fig. 5. (color online) Manual labeling of an image: the red mark (outer region), the grey mark (yellow spot), the yellow mark (optical disk).

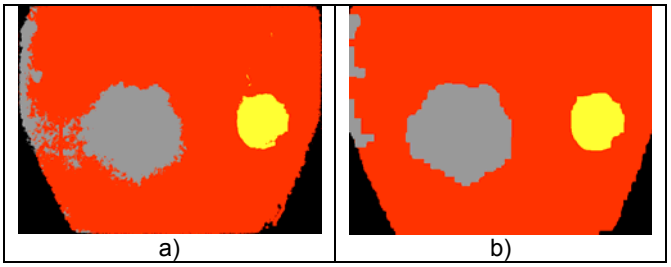


Fig. 6. (color online) The supervised segmentations: a) without postprocessing, b) with postprocessing.

The retina diagnosis methods presented in the literature, for fundus-camera eye-images, cannot fully rely on direct color features of images. In other words, the

spectral space of retina images in multispectral imaging is more discriminative in comparison to classical method. The presented segmentation algorithm will be improved by utilizing the local properties, and as we expect, that multispectral imaging will allow for more robust retina segmentation.

***Acknowledgement***

*This work was financed from the Polish Ministry of Science and Higher Education resources in 2009-2012 years as a research project*

REFERENCES

[1] Switonski A., Michalak M., Josinski H., Wojciechowski K., "Detection of tumor tissue based on the multispectral imaging" in *Computer Vision and Graphics. Lecture Notes in Computer Science*, R. Bieda Ed. (2010), pp. 325-333.

[2] Kruse F. A., "Use of airborne imaging spectrometer data to map minerals associated with hydrothermally altered rocks in the northern Grapevine Mountains, Nevada and California," Remote Sensing Environment 24, (1988), p. 31-51

[3] Lobo L. C., Ersoy O. K., Miles G. E., *Multispectral Imaging, Image-Processing and Classification for Agriculture,* Purdue University, Purdue e-Pubs, (2000).

[4] Imai F. H., Rosen M. R., Berns R. S., "Multi-spectral imaging of van Gogh's self-portrait at the National Gallery of Art, Washington, D.C.," *in Proceedings of Image Processing, Image Quality, Image Capturing System Conference* (The Society for Imaging Science and Technology, 2001) pp. 185-189.

[5]. Liu X., Wang D., Liu, F. Bai J., "Principal component analysis of dynamic fluorescence diffuse optical tomography images," Opt. Express 18, (2010), p. 6300-6314.

[6] Zhang X. Xu H., "Reconstructing spectral reflectance by dividing spectral space and extending the principal components in principal component analysis," J. Opt. Soc. Am. A 25, (2008), p. 371-378.

[7] Kim Y., "Incremental principal component analysis for image processing," Opt. Lett. 32, (2007), p 32-34.

[8]. Schölkopf B. Smola A., *Learning with Kernels. Support Vector Machines, Regularization, Optimization, and Beyond* (Massachusetts Institute of Technology, 2002).

[9] Schelkanova I., Toronov, V. " Independent component analysis of broadband near-infrared spectroscopy data acquired on adult human head," Biom. Opt. Express 3, (2011), p. 64-74.

[10] Kuan C.-Y. Healey G., "Using independent component analysis for material estimation in hyperspectral images," J. Opt. Soc. Am. A 21, (2008), p. 1026-1034.

[11] Vermeer K.A., van der Schoot J.,Lemij H. G., de Boer J. F., "Automated segmentation by pixel classification of retinal layers in ophthalmic OCT images," Biom. Opt. Express 2, (2011), p. 1743-1756.

[12].Chiu S. J., Toth C. A., Rickman C. B., Izatt J. A., Farsiu S., "Automatic segmentation of Closed-contour features in ophthalmic images using graph theory and dynamic programming," Biomed. Opt. Express 3, (2012), p. 1127-1140.

[13]. Yazdanpanah A., Hamarneh G., "Segmentation of intra-retinal layers from optical coherence tomography images using an active contour approach," IEEE Trans. Med. Imag. 30, (2011), p. 484-496.

[14]. Liu Y.-Y., Chen M., Ishikawa H., Wollstein G., Schuman J.S., Rehg J. M., "Automated macular pathology diagnosis in retinal OCT images using multi-scale spatial pyramid and local binary patterns in texture and shape encoding," Med. Image Anal. 15, (2011), p. 748-759.

[15]. Kokaram A.C., Persad N., Lasenby J., Fitzgerald W. J., McKinnon A., Welland M., "Restoration of images from the scanning-tunneling microscope," Appl. Opt. 34, (1995), p. 5121-5132.

[16]. Switoński A., Blachowicz T., Zieliński M., Josiński H., "Dimensionality reduction of multispectral images representing anatomical structures of an eye," *in Proceedings of the International MultiConference of Engineers and Computer Scientists* (IMECS 2012, March 14-16, Hong Kong), p. 740-745.

[17]. Witten I. Frank E., Data Mining: Practical Machine Learning. Tools and Techniques (*Morgan Kaufmann* Publishers, San Francisco, *2005)*.

[18]. Switonski A., Josinski H., Jedrasiak K., Polanski A.,. Wojciechowski K., "Classification of poses and movement phases," *in Proceedings of International Conference of Computer Vision and Graphics* (Lecture Notes in Computer Science, Springer, 2010), p. 193-200.

[19]. Michalak M. Switonski A., "Kernel Postprocessing of Multispectral Images Computer Recognition Systems," Comp. Reg. Sys. 4, (2011), p 395-401.

[20]. The Waikato Environment for Knowledge Analysis (WEKA) located at the University of Wakaito (New Zeland); http://www.cs.waikato.ac.nz/ml/weka/.

---

***Authors****: dr inż. Adam Świtoński,* Polish-Japanese Institute of Information Technology, Faculty of Bytom*, Aleja Legionów 2, 41-902 Bytom. E-mail aswitonski@pjwstk.edu.pl and* Silesian University of Technology, Faculty of Automatic Control, Electronics and Computer Science, ul. Akademicka 16, 44-100 Gliwice *E-mail adam.switonski@polsl.pl, prof. dr hab. inż. Tomasz Błachowicz,* Silesian University of Technology, Institute of Physics *ul. Bolesława Krzywoustego 2, 44-100 Gliwice, E-mail: tomasz.blachowicz@polsl.pl, prof. dr hab. Marta Misiuk Hojło Wrocław Medical University, Department of Ophthalmology, ul .Borowska 213, 50-530 Wrocław, prof. dr hab. Inż. Konrad Wojciechowski,* Polish-Japanese Institute of Information Technology, Faculty of Bytom*, Aleja Legionów 2, 41-902 Bytom. E-mail kwojecihowski@polsl.pl and* Silesian University of Technology, Faculty of Automatic Control, Electronics and Computer Science, ul. Akademicka 16, 44-100 Gliwice *E-mail konrad.wojciechowski@polsl.pl*